Journal of Nuclear Materials 585 (2023) 154630

Contents lists available at ScienceDirect

Journal of Nuclear Materials

journal homepage: www.elsevier.com/locate/jnucmat

Diffusion of small anti-Schottky clusters in UO_2

Andrew Garmon [a,*], Xiang-Yang Liu [b], David Andersson [b], Danny Perez [a]

[a] Theoretical Division, Los Alamos National Laboratory, Los Alamos, NM 87545, USA
[b] Materials Science and Technology Division, Los Alamos National Laboratory, Los Alamos, NM 87545, USA

ABSTRACT

The aggregation of irradiation-induced defect clusters in UO_2 leads to the formation of dislocation loops and cavities which contribute swelling and ultimately produce deleterious effects on the fuel. Despite their fundamental role in fuel evolution, the kinetics of these defect clusters are not currently well understood. In this work, we investigate the diffusive behavior of interstitial clusters via Molecular Dynamics (MD) simulations. Our investigation considers a range of defect cluster sizes, each composed of N UO_2 units or anti-Schottky defects. We report a complex cluster size - mobility relation; increasing cluster size corresponds to an increase in mobility up until a critical size ($N = 4$) where diffusivity reaches a maximum, after which the trend reverts and further increasing size corresponds to a decrease in mobility. The rapid migration observed correlates well with the very low barriers reported in a few historic experimental studies. Further analysis of the cluster shape and orientation reveals a strong structural preference for near-planar configurations oriented normal to the ⟨100⟩ direction. Rotational energy barriers are found to be similar in both magnitude and trend to the observed diffusion barriers. Lastly, connections are drawn to the behavior of large defect clusters including the formation of (1/3)⟨111⟩ Frank dislocation loops.

1. Introduction

The most commonly used material as a fuel in nuclear reactors is uranium dioxide (UO_2). As the fuel is irradiated during operation, irradiation-induced defect clusters tend to migrate and combine into increasingly large clusters and dislocation loops, which potentially contribute to fuel swelling and ultimately produce detrimental effects. In addition, the nucleation and growth of dislocation loops may influence the irradiation-induced point defect populations that interact with, e.g., fission gas atoms, and thus change their dynamics, which further impacts properties such as swelling and fission gas release. A more thorough understanding of the defect cluster kinetics is highly desirable, as it is the first step towards understanding, and eventually inhibiting or controlling, the nucleation and growth of these dislocation loops. It would also improve the ability to accurately predict fuel performance of existing and new UO_2-based fuel forms by improving mechanistic approaches to fuel performance modeling and in particular models related to fission gas dynamics [1,2]. This pursuit has remained challenging as direct experimental observation is difficult for very small clusters due to the limited resolution of, e.g., transmission electron microscopy (TEM). Experimental studies [3,4] have shown the formation of dislocation loops in UO_2 at low temperatures and estimate the migration barrier of U interstitials to be as low as 0.2 eV. This is intriguing as U interstitials are predicted to have much higher barriers [5], even when anti-Schottky defects are considered [6]. Furthermore, simulation studies [7] have found the migration barrier for O_2 interstitial clusters to be just as low, altogether alluding to the ubiquitous nature of this important physical phenomena. Dislocations are also known to play an important role in the formation of the so-called high-burnup structure that emerges in the periphery of UO_2 pellets upon extended irradiation [8].

Despite its importance, the transition from irradiation induced point defects to dislocation loops is not entirely well understood. Atomistic simulations are an ideal tool for studying the nucleation and growth of dislocation loops in UO_2. Work by Chartier et al. [9] has helped characterize the early stages of dislocation nucleation and growth under irradiation conditions. They found that irradiation induced dislocations followed a five stage process: (i) point defects are first created by irradiation, (ii) they aggregate into clusters, (iii) from which small Frank loops nucleate, (iv) which transform into unfaulted loops via the addition of Shockley partials that in turn grow, and (v) finally reorganize into forest dislocations. These simulations used the Frenkel pair accumulation methodology to mimic ballistic damage. Using displacement cascades, Balboa et al. observed the same process including the transformation of Frank loops into unfaulted loops [10]. Similarly, Martin et al. used 10 keV displacement cascades to study defect nucleation and observed similar physical behavior [11].

* Corresponding author.
E-mail address: agarmon@lanl.gov (A. Garmon).

https://doi.org/10.1016/j.jnucmat.2023.154630
Received 4 May 2023; Received in revised form 28 June 2023; Accepted 11 July 2023
Available online 18 July 2023

Although these studies have helped provide insight into the formation of dislocation loops in UO_2 they have focused on collision cascades as the underlying means of production. In practice however, irradiation damage is known to occur as two distinct phases: a quick (∼ ps) ballistic phase and a slow (∼ ns-μs) kinetic phase. During the ballistic phase, a collision cascade produced by high-energy particles creates points defects. During the kinetic phase, thermal diffusion and recombination leads to the formation of extended defect clusters. Although collision cascade simulations can capture the physics of the ballistic phase, they are not informative of the kinetic phase. This is important as other simulations (e.g., Uberuaga et al. [12]) have found that the evolution of defects into extended defects is oftentimes independent of the detailed nature of the ballistic phase, thereby suggesting that the importance of the ballistic phase is mostly in introducing point defects into the system.

Small interstitial clusters are hence considered as basic units in formation of the interstitial dislocation loops. Understanding of the evolution kinetics of these interstitial clusters is useful for upscaling atomistic information into mesoscale models such as cluster dynamics [13]. As shown earlier, introduction of anti-Schottky defect in cluster dynamics models of UO_2 plays an important role in controlling point defect concentrations [13].

In this work, we explore the kinetic behavior of small interstitial defect clusters to better understand how they diffuse and combine, thereby identifying the conditions required for dislocation loops to form. The recent work of Liu and Andersson [14] serves as our motivation, as they examined the kinetics of very small UO_2 interstitial clusters through the use of an accelerated molecular dynamics (MD) method. They considered clusters comprised of N UO_2 interstitial units (anti-Schottky defect clusters), $N = \{1, 2, 3\}$. Their work found the mobility of interstitial clusters to increase with the size of the cluster; a perhaps non-intuitive result. Our work, as described below, has been carried out to extend our understanding of the relation between interstitial cluster size, structure, and mobility to a broader range of cluster sizes.

1.1. Methods

Our work utilizes a set of MD simulations that were performed using the interatomic potential developed by Morelon et al. [15] which was designed for simulating the formation and mobility of defects in UO_2. More specifically, it was fitted to reproduce experimental defect formation and migration energies. It has also been shown to describe some more basic properties of UO_2, such as thermal expansion coefficient and heat capacity, over a large range of temperatures [16,17]. This potential was also used in the motivating work [14] and is believed to give a good qualitative description of systematic trends.

Each simulation was run in the canonical NVT ensemble with a Langevin thermostat using a damping parameter of 0.01 ps. These simulations were carried out with the parallel MD code LAMMPS [18] using periodic boundary conditions and a timestep of 1 fs. Expanding upon the motivating work, we chose to investigate interstitial clusters consisting of N UO_2 units or anti-Schottky defects. Each atomic configuration was constructed from an initial cell of bulk UO_2 consisting of $8 \times 8 \times 8$ UO_2 unit cells, measuring roughly 44 Å in each direction. This volume was selected as it was observed to be large enough to model interstitial cluster diffusion without any finite size effects for a cluster size of $N = 7$ UO_2 units. A compact 3D cluster of N UO_2 units was randomly inserted near the center of the cell and then briefly annealed for 10 ps at 500 K before quenching to obtain a locally stable minimum energy structure (Fig. 1). For each cluster size (N), a single initial configuration was created in this way. The Wigner-Seitz defect analysis from Ovito [19] was utilized throughout this work to identify the location of the interstitial defects with respect to the initial bulk UO_2 cell.

Clusters ranging in size from $N = \{1 - 7\}$ were studies at temperatures ranging from 1000 K to 1600 K in 100 K intervals. For each cluster size and temperature, a single very-long MD simulation of several hundred nanoseconds was carried out. The resulting trajectories were analyzed to assess whether the interstitial cluster broke into smaller clusters during the simulation. This was done by verifying that the U interstitial atoms formed a single cluster as defined by a cutoff region of 8 Å. The location of the O interstitial atoms was also monitored, as reported below.

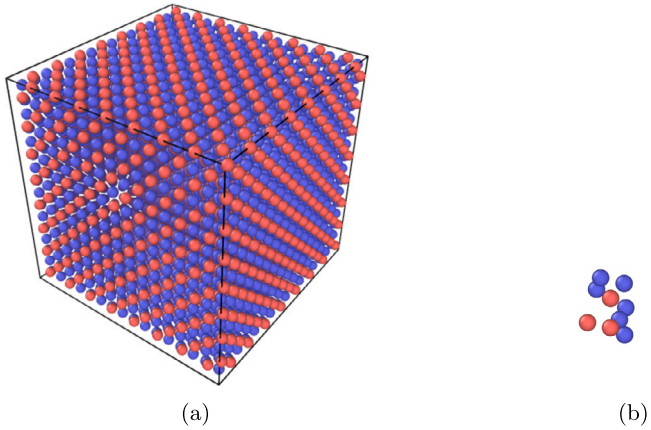

Fig. 1. Each atomic configuration was constructed from an initial cell consisting of $8 \times 8 \times 8$ UO_2 unit cells, measuring roughly 44 Å in each direction (a), into which a cluster of N UO_2 interstitials were inserted and annealed, shown here for example (b) $N = 3$. Atoms are shown here colored by type with U atoms in red and O atoms in violet. (For interpretation of the colors in the figure(s), the reader is referred to the web version of this article.)

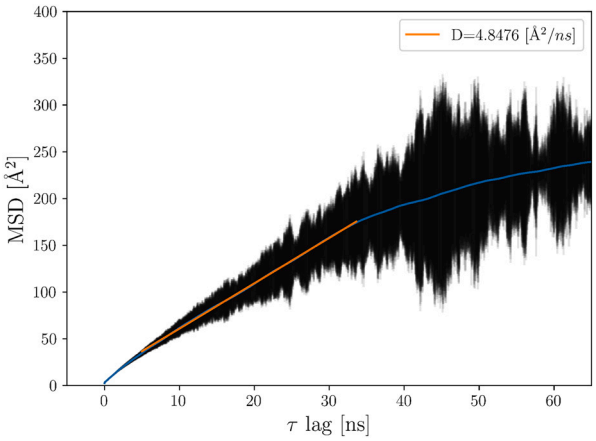

Fig. 2. MSD for the $N = 4$ interstitial clusters at $T = 1500$ K with bootstrap standard error of the mean (SEM) error-bars. The linear diffusion region, shown in orange, was used to infer a diffusion coefficient of roughly 4.85 Å²/ns in this case.

The atomic trajectories were used to compute the Mean Squared Displacement (MSD) of the center of mass of the interstitial cluster over a varying lag-time. To eliminate the noise caused by O interstitials that constantly detach and rejoin the cluster, the MSD was computed from the center of mass of the U interstitials alone, as they always remained bound and therefore better defined the location of the interstitial cluster. For each cluster size and temperature, a diffusion coefficient was extracted from the 'linear region' of the MSD which was identified using a method [20] to analytically determine upper and lower bound values for the linear diffusion region (Fig. 2). To ensure that our simulations were in a normal diffusion regime and not in a transient sub-diffusion regime we analyzed the square root of the MSD to find that center-of-mass displacements exceed a few lattice constants. An Arrhenius plot was then constructed with the diffusion coefficient data to extract diffusion energy barriers and exponential pre-factors. In simulations where the motion of the cluster was limited to just a handful of jumps the

bootstrap procedure we employ results in very large error bars (as some sub-sets of the data show no diffusion while others do). The error bars therefore give an informative indication of the "borderline" cases where the simulations are at the boundary between the diffusive and sub-diffusive regimes.

2. Results

In monitoring the location of the O interstitial atoms, it was observed that $N = 1$ cluster does not remain bound at even the lowest temperatures in our study. As a result, the $N = 1$ cluster data was omitted as the diffusive behavior observed was more accurately describing some combination of a $N = 1$ cluster and a single U interstitial. The remaining small cluster simulations reproduced the same qualitative behavior observed in the motivating work; the $N = 3$ interstitial cluster diffuses far more rapidly than the smaller $N = 2$ cluster over a range of temperatures. This trend of increased mobility with increasing cluster size continued to include the $N = 4$ cluster, which was found to diffuse quite rapidly even at the lowest temperatures studied. However, this trend is shown to reverse after $N = 4$, as mobility decreased for $N = \{5, 6, 7\}$, with the $N = 7$ cluster showing very little diffusivity on MD-accessible timescales.

Fig. 3 shows the Arrhenius fits ($D = D_0 \exp[-E_a/K_b T]$) of the diffusion coefficients for each cluster size, enabling us to extract the diffusion energy barriers (E_a) and pre-exponential factors (D_0). The $N = 4$ cluster was found to have a remarkably low diffusion energy barrier of just 0.317 eV, less than half the value of the next lowest energy barrier (the $N = 6$ cluster with an energy barrier of 0.64 eV) and less than one third the value of the highest energy barriers ($N = 2$ cluster with a 0.999 eV energy barrier and the $N = 7$ cluster with a 1.099 eV energy barrier). The small range of cluster sizes yielded an order of magnitude difference in diffusion coefficients (Fig. 4). Although there is a definite trend in cluster mobility, the $N = 4$ cluster stands out among the rest with its rapid diffusivity. Note how the addition or removal of just a few UO_2 units results in dramatically higher diffusion energy barriers. As shown in Fig. 5, this system provides an example of the Meyer-Neldel rule [21] as the effect of high barriers is partially offset by high prefactors. Most of the cluster sizes have prefactors greater than an order of magnitude higher than the $N = 4$ cluster. Nonetheless, the $N = 4$ cluster still exhibits the highest diffusivity overall. The energy barrier trend shows that as small interstitial clusters migrate and combine to form larger clusters, there will be an increase in mobility up to a critical size where further growth will result in decreased mobility. Given that defect clusters may break apart before growing by merging with other clusters, we cannot draw definitive conclusions regarding evolution of the population of different defects based on the diffusion kinetics alone.

Migration barriers for interstitial clusters can be smaller than that of mono-interstitials, e.g., in pure metals [22,23] as well as oxides like MgO [12] and UO_2 [7]. In pure metals, self-interstitial atoms (SIAs) can form glissile dislocation loops, which can diffuse rapidly in 1D along the crowdion direction. Since the general diffusion mechanism remains the same, the migration barrier does not change drastically with cluster size. This is not the case with the UO_2 clusters. Not only is a large range in barrier heights observed, the UO_2 interstitial clusters are found to diffuse freely in three dimensions. Our results are more similar to that of metal oxides like those investigated in Bai et al. [7] who found oxygen interstitial clusters (O_i) to possess a unique migration barrier ordering ($O_2 < O_3 < O_1 < O_5 < O_4$). This is in comparison to our anti-Schottky interstitial clusters ($U_N\ O_{2N}$, comprised of N units of UO_2) which were found to have a diffusion barrier ordering: $N = 4 < N = 6 < N = 5 < N = 3 < N = 2 < N = 7$, with pre-exponential factors following a very similar ordering. In further similarity to the oxygen interstitial clusters, we found the lowest energy barrier ($N = 4$ cluster) to be several times lower than the other barrier heights studied, just as Bai et al. found with the O_2 cluster [7]. This illustrates another example where native interstitial clusters in UO_2 can exhibit such a large range of energy barriers over a small range in cluster size.

The shape of each cluster was characterized by computing the semi-axes of an equivalent ellipsoid as derived from the moment of inertia tensor [24]. These values are denoted by U_1, U_2, and U_3. For example, a cluster with a single non-zero U-value is completely linear, having zero width along two of its principles axes. Conversely, a cluster having three U-values of equal magnitude would describe an isotropic spherical cluster. One might expect small defect clusters to be of this second type, however our simulations show that even at low N these defect clusters tend to show some level of shape anisotropy, i.e., the larger defect clusters ($N = \{5, 6, 7\}$) prefer near-planar configurations characterized by two U-values that are much greater than the third. Shown in Fig. 6, the $N = 7$ defect cluster has a flat 'pancake-like' structure corresponding an oblong ellipsoid. The direction of the smallest U-value, illustrated in the figure by the red vector, can be used to help quantify the orientation of the defect cluster throughout the simulation.

In analyzing the timeseries of U-values throughout a simulation we found there to exist a short initial transient of a few ns where the shape of the cluster equilibrates, after which the U-values fluctuate for the remainder of the simulation. This is representative of the relaxation of the initial random configuration towards an equilibrated configuration, followed by the sampling of the different metastable states of the cluster. This same behavior was observed in all cases we explored, strongly suggesting that the shape of the initial configuration does not significantly affect the configurations observed during the simulations.

For each long-time MD trajectory the direction corresponding to the smallest U-value, hereby referred to as Θ, was computed as a function of time. Analysis of $\Theta(t)$ founds there to be a preferred crystallographic orientation for each of the larger defect clusters ($N = \{5, 6, 7\}$) along the $\langle 100 \rangle$ direction. The density contour plots in Fig. 7 show the distribution of $\Theta(t)$ in terms of the equivalent crystallographic direction. As can be seen in Fig. 7a for the $N = 7$ cluster, $\Theta(t)$ is very densely oriented along the $\langle 100 \rangle$ direction with the remaining frames orientated almost uniformly. Given that Θ corresponds to the direction normal to the plane of a near-planar configuration, it implies that the defect clusters not only prefer compact pancake-like configurations, but they also tend to orient along the same crystallographic plane. This is an important feature as it pertains to the formation dislocation loops that will be discussed later.

One may note that the Morelon potential, like many other pair potentials, does not reproduce the Cauchy violation and behaves nearly isotropic in the elastic properties of UO_2. However, this drawback in the description of the elastic properties does not necessarily translate to a direct impact on the cluster crystallographic orientation preference found here. In other nearly isotropic materials, like tungsten (W), the self-interstitial-atom based clustering also grows into crystallographic oriented dislocation loops, where the isotropic elasticity of W does not prevent the occurrence of such phenomena [25].

Deriving $\Theta(t)$ enabled the construction of a orientational autocorrelation function $\langle |\Theta(t)\Theta(t+\tau)| \rangle_t$, where the angled bracket represents an ensemble average over all time t. The correlation function begins at an initial value of 1 at short times and then gradually decays down to a minimum value of 0.5, which corresponds to the autocorrelation of two random vectors sampled on a sphere. The decay of the autocorrelation contains at least two characteristic timescales; a fast decay caused by the local thermal motion and a slower decay capturing the rotational diffusion, i.e., the reorientation of the cluster along a different direction. To capture these two characteristic timescales, the decay of each autocorrelation function was fit to the sum of two exponential functions constrained to sum to 1 at $\tau = 0$ and to decay to 0.5 at long times, taking the functional form $0.5\frac{a\exp[-bt]+c\exp[-dt]}{a+c} + 0.5$. This correlation function is illustrated in Fig. 8 for the $N = 7$ cluster at $T = 1300$ K where the diffusion coefficient is found to be $d = 0.426\ \text{ns}^{-1}$.

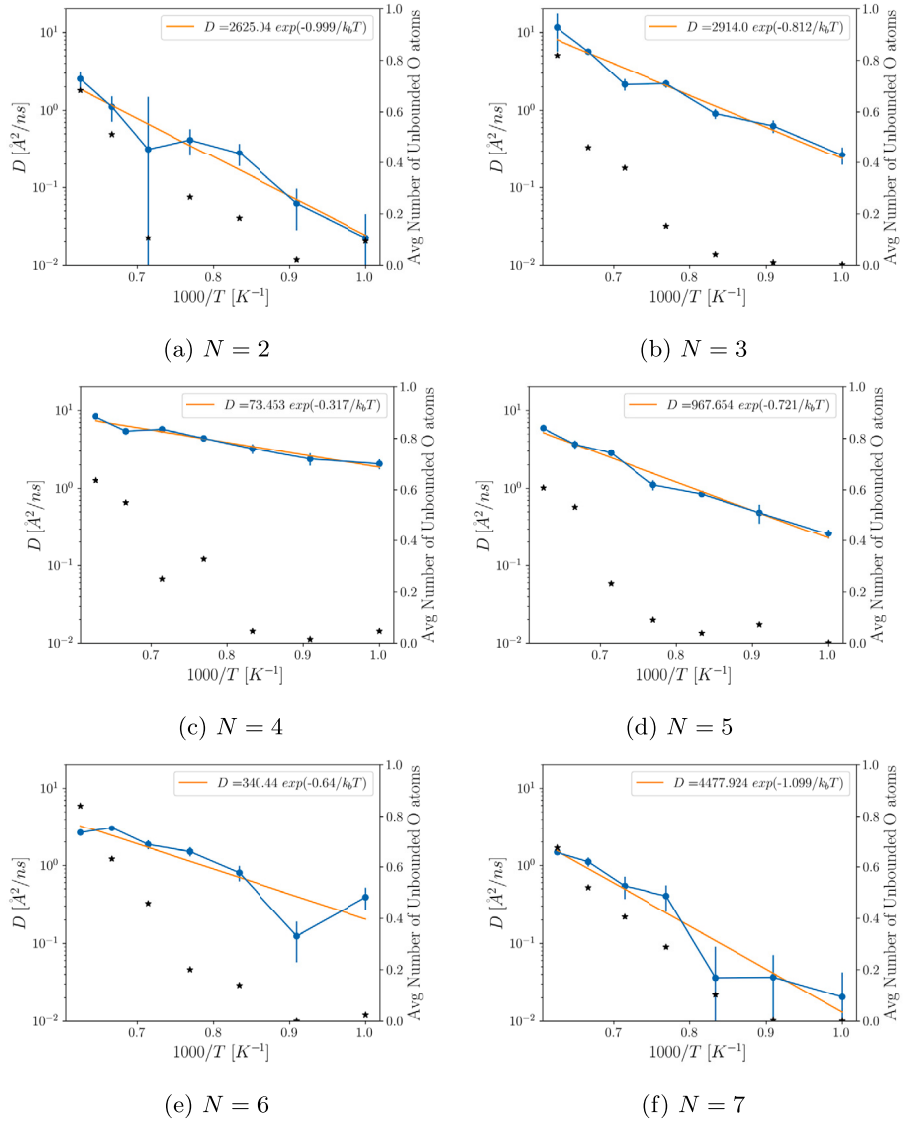

Fig. 3. Diffusivity of the different interstitial clusters. Each blue point corresponds to a single MD run from which the diffusion coefficient was extracted. An Arrhenius fit was then used to estimate the diffusion energy barriers and exponential pre-factors. The black stars correspond to the second vertical axis (right side) showing the average number of O atoms that were not bound to the cluster throughout the simulation. It can be seen that despite there being $2N$ O interstitial atoms in each simulation, the average number of unbounded O interstitials was less than 1 for each simulation.

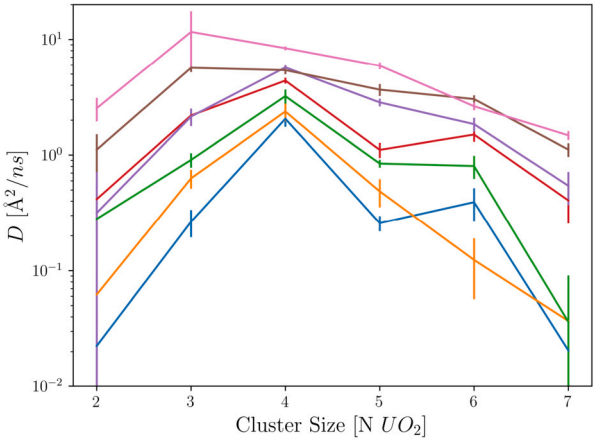

Fig. 4. Diffusion coefficients as a function of cluster size (N) shown for the range of temperatures [1000 K (blue), 1100 K (orange), 1200 K (green), 1300 K (purple), 1400 K (red), 1500 K (brown), and 1600 K (pink)] with 1 standard deviation confidence intervals.

Fig. 9 shows the Arrhenius fits ($D = D_0 \exp[-E_a/K_bT]$) of the rotational diffusion coefficients for the $N = \{5, 6, 7\}$ cluster sizes, allowing us to extract the rotational energy barriers (E_a) and pre-exponential factors (D_0). The barrier heights observed are fairly high and suggest that these larger clusters are strongly orientationally stable. The smaller cluster sizes ($N = \{2, 3, 4\}$) are not shown, as shape fluctuations were there too fast to discern any diffusive behavior. As can be seen in Fig. 10, the rotational energy barriers are consistent with the observed diffusion barriers. The close similarities in barrier heights, both in magnitude and in trend, suggest that rotation and diffusion are likely intimately linked and that rotation might be necessary in order for the cluster to migrate. This is in contrast to pure metals where one dimensional diffusion readily occurs and rotations are infrequent [23,26–28]. In even greater contrast, although the rotation energy barriers in pure metals can be more than twice the diffusion energy barriers [23], these barriers are an order of magnitude lower than the barriers observed in our study, thereby further indicating that the UO_2 interstitial clusters are significantly more orientationally stable than SIA clusters in metals.

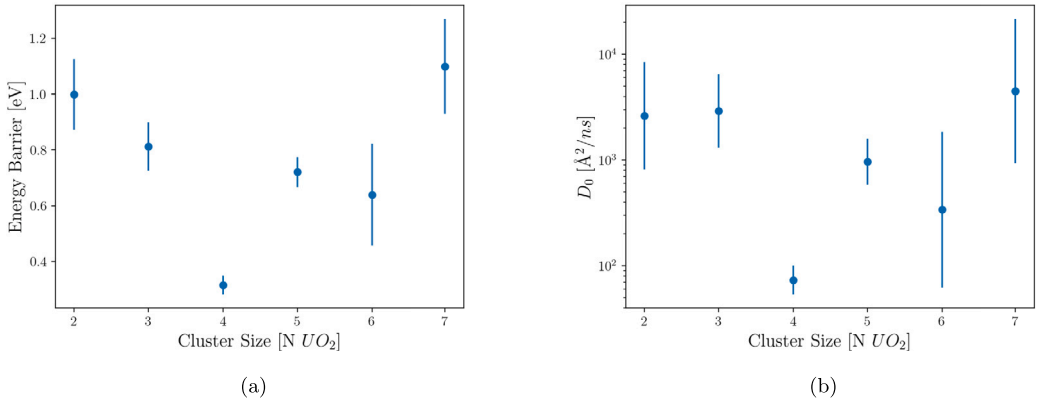

Fig. 5. (a) Diffusion energy barriers and (b) Pre-exponential factors shown as a function cluster size (N) with 1 standard deviation confidence intervals.

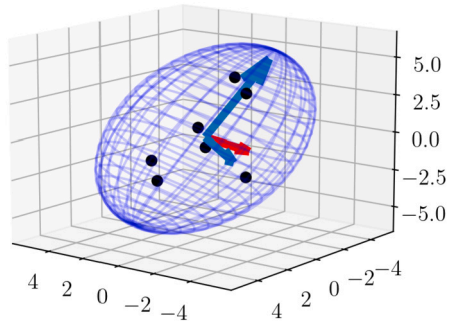

Fig. 6. The $N = 7$ defect clusters encapsulated by the equivalent ellipsoid as shown with semi-axes vectors. The red vector denotes the direction perpendicular to the flattest region of the cluster corresponding to the smallest U-value. The U-values for this configuration were 2.35 Å, 4.55 Å, and 5.73 Å.

In addition to our small cluster analysis, we conducted high temperature ($T = 1800$ K) simulations of large ($N = \{10, 12, 14, 16\}$) defect clusters out to several hundred nanoseconds. The $N = 16$ cluster simulation showed the formation of a Frank $(1/3)\langle 111\rangle$ dislocation loop roughly 10 ns into the simulation, which then remained stable for the entire 500 ns simulation. While the center of mass of the defect cluster showed small variability during the first 10 ns, it showed no variation after the dislocation loop was formed. This shows that the formation of Frank loops helps lock the defect cluster into place and inhibits further migration. In contrast, the smaller defect clusters were not observed to form a *stable* dislocation loop. Meanwhile, the mobility of these defect clusters (albeit quite small) exhibited an inverse trend with size, further suggesting that the formation of a dislocation loop may considerably slow down the cluster motion.

In relation to our small cluster analysis which showed a preferred Θ orientation along the $\langle 100\rangle$ direction, these larger clusters exhibited a progressive transition from a preferred $\langle 100\rangle$ direction toward a $\langle 111\rangle$ direction. This transition is visually captured in Figs. 7b-7e. The $N = 10$ cluster shows a wide spread in Θ as compared to the smaller clusters but is still centered around the $\langle 100\rangle$ direction. The $N = 12$ and $N = 14$ clusters exhibit an even greater spread, with densest region of the $N = 14$ cluster having shifted from the $\langle 100\rangle$ to the $\langle 111\rangle$ direction. Lastly, the $N = 16$ cluster is firmly aligned in the $\langle 111\rangle$ direction after the Frank $(1/3)\langle 111\rangle$ dislocation loop is formed. This transition in Θ orientation from $\langle 100\rangle$ to $\langle 111\rangle$ with increasing cluster size increases has been observed in pure metal systems. Osetsky et al. found that copper SIAs exists in small stable clusters oriented along the $\langle 100\rangle$ direction which, during growth, transformed into faulted Frank $(1/3)\langle 111\rangle$ dislocation loops [23]. It is interesting that they share similar structural properties given the fundamental differences in mobility behavior: our small clusters exhibited three dimensional mobility with rotation and diffusion energy barriers of similar magnitude and transformed under growth to produce sessile Frank $(1/3)\langle 111\rangle$ dislocation loops. This is in contrast to pure metals that exhibit one dimensional fast glide along the crowdion direction and occasional rotations to equivalent directions.

3. Conclusions

In this work, we analyzed the kinetic behavior of small interstitial clusters comprised of N UO_2 interstitial units (anti-Schottky defect clusters). We examined clusters of size $N = 2$ to $N = 7$ over a range of temperatures (1000 K to 1600 K). Each simulation was used to calculate a diffusion coefficient from the MSD of the center of mass of the uranium interstitial atoms. Using an Arrhenius fit of the data, we extracted diffusion energy barriers as well as pre-exponential factors for each cluster size. Our calculations successfully reproduced the small cluster results of Liu and Andersson, finding the $N = 3$ cluster to have greater mobility than the $N = 2$ cluster. Our work found this trend of increased mobility with increased cluster size to include the $N = 4$ cluster which had the lowest diffusion energy barrier of 0.317 eV. For clusters of greater size this trend began to reverse showing decreased mobility and higher diffusion energy barriers with increased size. Our results were therefore able to capture the full extent of the cluster size - mobility relation, identifying the turning point where increasing cluster size begins to decrease mobility.

We then further examined the interstitial clusters to characterize the cluster shape. It was found that the small defect clusters tend to exhibit some degree of anisotropy in their shape, namely flat pancake-like structures oriented normal to the $\langle 100\rangle$ direction. This was congruent with larger cluster simulations that showed a transition in orientation from the $\langle 100\rangle$ direction to the $\langle 111\rangle$ direction. The largest of theses simulations ($N = 16$) observed the formation of a stable sessile Frank $(1/3)\langle 111\rangle$ dislocation loop as has been observed in the literature. We constructed orientational autocorrelation functions of the small cluster data and fit them to decaying exponential functions to extract a rotational diffusion coefficient. A similar trend which was found to exist for cluster diffusion was shown to exist for cluster rotation, suggesting that rotation and diffusion may be directly connected. Our work helped identify a complex cluster size - mobility relation; increasing cluster size corresponds to an increase in mobility up until a critical size ($N = 4$) where diffusivity reaches a maximum, after which the trend begins to reverse and further increasing size corresponds to decreased mobility. This complex relationship provides insight into the formation process of large, immobile interstitial clusters. Providing an understanding for the origin of these larger clusters is of great importance as they relate to the formation of dislocation loops. The next steps in building upon this understanding are probing the formation and growth of dislocation loops based on these UO_2 interstitial clusters.

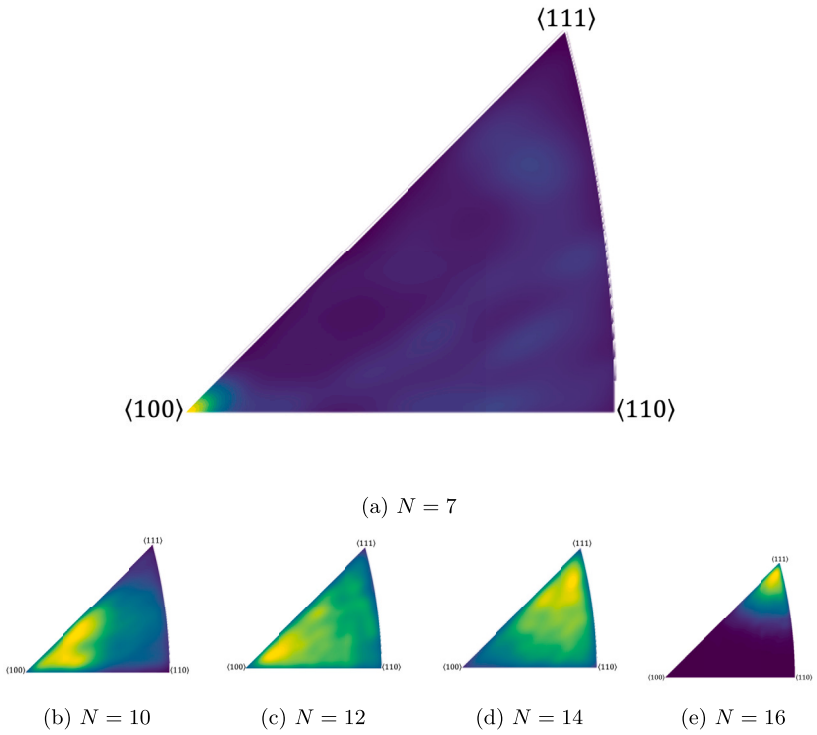

Fig. 7. Density contour plots showing the distribution of $\Theta(t)$ in terms of the equivalent crystallographic direction. Each plot was constructed from 300 ns of MD trajectory with the atomic configuration analyzed every 10 ps resulting in 30,000 data points. The density is illustrated using a linear color scale with the brightest regions representing the greatest density. Fig. 7a was constructed from a $T = 1500$ K simulation and Figs. 7b-7e were constructed from $T = 1800$ K simulations.

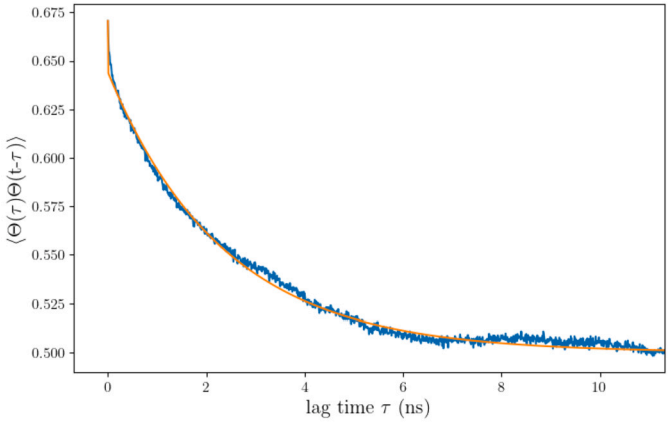

Fig. 8. Directional autocorrelation function of the smallest U-value direction. Shown here for the $N = 7$ interstitial clusters at $T = 1300$ K. The rotational diffusion coefficient for this system found to be roughly 0.426 ns^{-1}.

CRediT authorship contribution statement

Andrew Garmon: Conceptualization, Data curation, Formal analysis, Investigation, Visualization, Writing – original draft. **Xiang-Yang Liu:** Conceptualization, Writing – review & editing. **David Andersson:** Conceptualization, Funding acquisition, Writing – review & editing. **Danny Perez:** Conceptualization, Formal analysis, Project administration, Writing – review & editing.

Declaration of competing interest

The authors declare the following financial interests/personal relationships which may be considered as potential competing interests: Andrew Garmon reports financial support was provided by US Department of Energy Office of Nuclear Energy. Danny Perez reports financial support was provided by US Department of Energy.

Data availability

Data will be made available on request.

Acknowledgements

This work was supported by the U.S. Department of Energy Office of Nuclear Energy and Office of Science, Office of Advanced Scientific Computing Research through the Scientific Discovery through Advanced Computing project on Simulation of Fission Gas Simulation of Fission Gas in Uranium Oxide Nuclear Fuel. D.P. was supported by the Exascale Computing Project (17-SC-20-SC), a collaborative effort of the US Department of Energy Office of Science and the National Nuclear Security Administration. Los Alamos National Laboratory is operated by Triad National Security LLC, for the National Nuclear Security administration of the U.S. DOE under Contract No. 89233218CNA0000001. We graciously acknowledge computing resources from the Los Alamos National Laboratory Institutional Computing (IC) program.

References

[1] Michael W.D. Cooper, Giovanni Pastore, Yifeng Che, Christopher Matthews, Axel Forslund, Christopher R. Stanek, Koroush Shirvan, Terje Tverberg, Kyle A. Gamble, Brian Mays, David A. Andersson, Fission gas diffusion and release for Cr_2O_3-doped UO_2: from the atomic to the engineering scale, J. Nucl. Mater. 545 (2021) 152590.

[2] Dong-Uk Kim, Sophie Blondel, David E. Bernholdt, Philip Roth, Fande Kong, David Andersson, Michael R. Tonks, Brian D. Wirth, Modeling mesoscale fission gas behavior in UO_2 by directly coupling the phase field method to spatially resolved cluster dynamics, Mater. Theory 6 (7) (2022).

[3] J. Soullard, High voltage electron microscope observations of UO_2, J. Nucl. Mater. 135 (2–3) (1985) 190–196.

[4] A.D. Whapham, B.E. Sheldon, Radiation damage in uranium dioxide, Philos. Mag. 12 (120) (1965) 1179–1192.

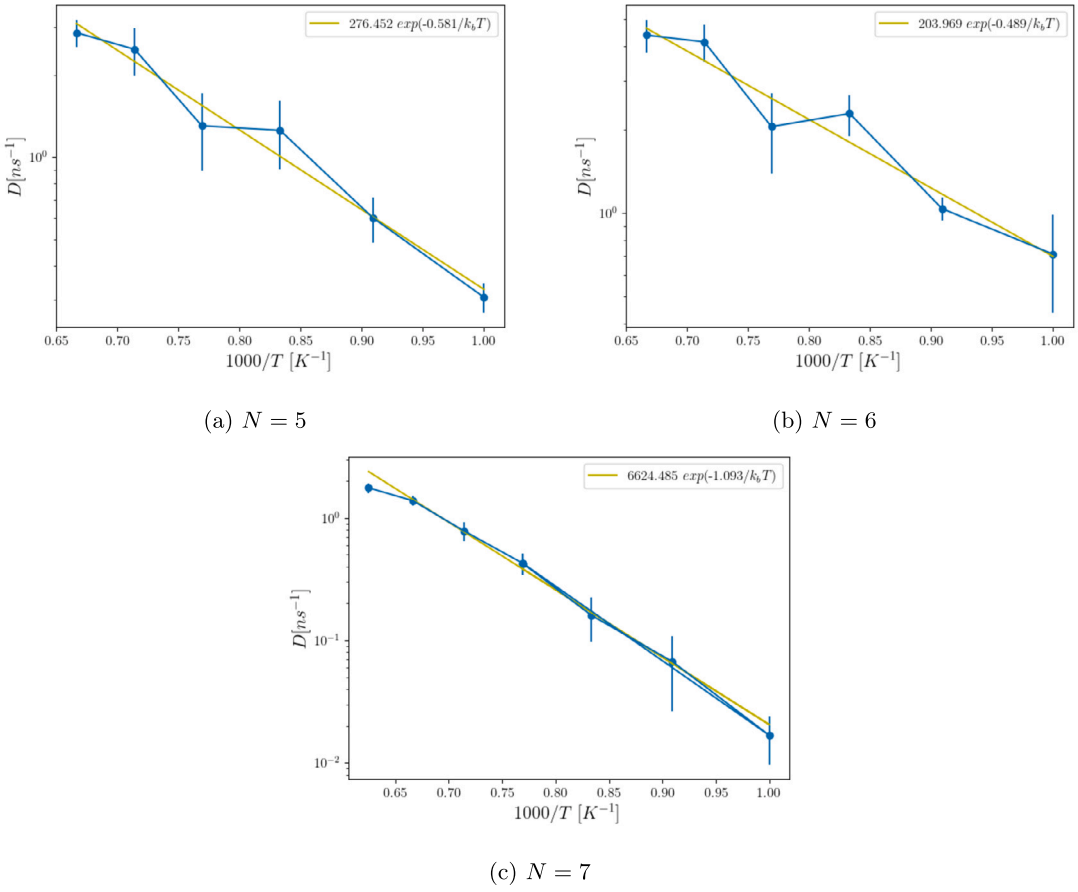

Fig. 9. Rotational diffusivity of the $N = \{5, 6, 7\}$ interstitial clusters with bootstrap standard error of the mean (SEM) error-bars. Each blue point corresponds to a single MD run from which the diffusion coefficient was extracted. An Arrhenius fit was then used to estimate the diffusion energy barrier and exponential pre-factors.

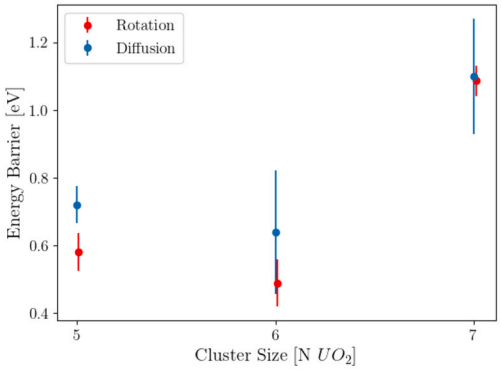

Fig. 10. Relation between diffusion and rotation energy barriers with 1 standard deviation confidence intervals. The rotation energy barriers (red) have been slightly offset for visibility.

[5] Boris Dorado, David A. Andersson, Christopher R. Stanek, Marjorie Bertolus, Blas P. Uberuaga, Guillaume Martin, Michel Freyss, Philippe Garcia, First-principles calculations of uranium diffusion in uranium dioxide, Phys. Rev. B 86 (Jul 2012) 035110.

[6] Christopher Matthews, Romain Perriot, Michael W.D. Cooper, Christopher R. Stanek, David A. Andersson, Cluster dynamics simulation of uranium self-diffusion during irradiation in UO_2, J. Nucl. Mater. 527 (2019) 151787.

[7] Xian-Ming Bai, Anter El-Azab, Jianguo Yu, Todd R. Allen, Migration mechanisms of oxygen interstitial clusters in UO_2, J. Phys. Condens. Matter 25 (1) (2012) 015003.

[8] Hj. Matzke, M. Kinoshita, Polygonization and high burnup structure in nuclear fuels, J. Nucl. Mater. 247 (1997) 108–115, Thermodynamics of Nuclear Materials.

[9] A. Chartier, Claire Onofri, L. Van Brutzel, Ch Sabathier, O. Dorosh, J. Jagielski, Early stages of irradiation induced dislocations in Urania, Appl. Phys. Lett. 109 (18) (2016) 181902.

[10] Damage characterization of (U,Pu)o.

[11] G. Martin, Ph Garcia, C. Sabathier, L. Van Brutzel, B. Dorado, F. Garrido, S. Maillard, Irradiation-induced heterogeneous nucleation in uranium dioxide, Phys. Lett. A 374 (30) (2010) 3038–3041.

[12] B.P. Uberuaga, Roger Smith, A.R. Cleave, F. Montalenti, G. Henkelman, R.W. Grimes, A.F. Voter, K.E. Sickafus, Structure and mobility of defects formed from collision cascades in MgO, Phys. Rev. Lett. 92 (11) (2004) 115505.

[13] C. Matthews, R. Perriot, M.W. Cooper, C.R. Stanek, D.A. Andersson, Cluster dynamics simulation of uranium self-diffusion during irradiation in UO_2, J. Nucl. Mater. 527 (2019) 151787.

[14] X-Y. Liu, D.A. Andersson, Small uranium and oxygen interstitial clusters in UO_2: an empirical potential study, J. Nucl. Mater. 547 (2021) 152783.

[15] N-D. Morelon, D. Ghaleb, J-M. Delaye, L. Van Brutzel, A new empirical potential for simulating the formation of defects and their mobility in uranium dioxide, Philos. Mag. 83 (13) (2003) 1533–1555.

[16] Kevin Govers, Sergei Lemehov, Marc Hou, Marc Verwerft, Comparison of interatomic potentials for UO_2. part I: static calculations, J. Nucl. Mater. 366 (1–2) (2007) 161–177.

[17] Kevin Govers, Sergei Lemehov, Marc Hou, Marc Verwerft, Comparison of interatomic potentials for UO_2: part II: molecular dynamics simulations, J. Nucl. Mater. 376 (1) (2008) 66–77.

[18] Steve Plimpton, Fast parallel algorithms for short-range molecular dynamics, J. Comput. Phys. 117 (1) (1995) 1–19.

[19] Alexander Stukowski, Visualization and analysis of atomistic simulation data with ovito–the open visualization tool, Model. Simul. Mater. Sci. Eng. 18 (1) (2009) 015012.

[20] Xingfeng He, Yizhou Zhu, Alexander Epstein, Yifei Mo, Statistical variances of diffusional properties from ab initio molecular dynamics simulations, npj Comput. Mater. 4 (1) (2018) 1–9.

[21] Ghyslain Boisvert, Laurent J. Lewis, Arthur Yelon, Many-body nature of the Meyer-Neldel compensation law for diffusion, Phys. Rev. Lett. 75 (3) (1995) 469.

[22] N. Soneda, T. Diaz de La Rubia, Migration kinetics of the self-interstitial atom and its clusters in BCC Fe, Philos. Mag. A 81 (2) (2001) 331–343.

[23] Yu N. Osetsky, D.J. Bacon, A. Serra, B.N. Singh, S.I. Golubov, Stability and mobility of defect clusters and dislocation loops in metals, J. Nucl. Mater. 276 (1–3) (2000) 65–77.

[24] Frédéric Gruy, Inertia tensor as morphological descriptor for aggregation dynamics, Colloids Surf. A, Physicochem. Eng. Asp. 482 (2015) 154–164.
[25] Pui-Wai Ma, D.R. Mason, S.L. Dudarev, Multiscale analysis of dislocation loops and voids in tungsten, Phys. Rev. Mater. 4 (10) (2020) 103609.
[26] Luis A. Zepeda-Ruiz, Jörg Rottler, Brian D. Wirth, Roberto Car, David J. Srolovitz, Self-interstitial transport in vanadium, Acta Mater. 53 (7) (2005) 1985–1994.
[27] Yu N. Osetsky, M. Victoria, A. Serra, S.I. Golubov, V. Priego, Computer simulation of vacancy and interstitial clusters in bcc and fcc metals, J. Nucl. Mater. 251 (1997) 34–48.
[28] R.C. Pasianot, A.M. Monti, G. Simonelli, E.J. Savino, Computer simulation of sia migration in bcc and hcp metals, J. Nucl. Mater. 276 (1–3) (2000) 230–234.